URSI, Boulder, Jan 2005

Real Time Imaging

Melvyn Wright

Radio Astronomy Laboratory, University of California, Berkeley, CA, 94720

ABSTRACT

. Calibration and imaging integrated with hardware.
. Stream data processing
. Calibration in real time using global model.
. Calibration feedback into beam formers and imagers.
. Simultaneous imaging at multiple phase centers.
. Calibrated images as normal output.

1. Acknowledgements

The students who participated in my imaging seminar. Don Backer for opportunity to work on EoR data. Gerry Harp for turning my pencil drawing into Figure 1. Udaya Shankar for a careful reading of SKA memo 60. Dan Werthimer and the BEE group at BWRC.

2. MOTIVATION for REAL TIME IMAGING

. Primary interest is astronomy, not data processing.

. Telescope use by non experts.

. Severe mismatch between on-line and off-line data rates.

. Non coplanar array geometry

. Non isoplanicity of atmosphere.

. Sources in the sidelobes of the primary beam.

. Primary beam is time variable

. Transient sources.

. Targets of opportunity.

. RFI handled as the data are acquired.

. Delayed calibration and analysis limit science.

. Off-line data reduction expensive and time consuming.

. Expertize many astronomers do not have or want.

. Best use of telescope and human resources.

. Calibrated images as normal output.

3. System Architecture and Data Processing Model.

3.1. Digitize

. Total analog bandwidth $N \times B \times N_{pol}$.

. The total data bandwidth is $N \times 2B \times N_{pol} \times N_{bits}$,

4 10^{12} $(N/1000)$ $(N_{pol}/2)$ (B/GHz) $(N_{bits}/8)$ bytes/s

3.2. Channelize

. Large N, high dynamic range favors FX design.

— spectral resolution,

— bandwidth smearing

— RFI mitigation

. Polyphase filter.

— Excellent channel separation.

— Full bit growth.

— 4-bit selection.

— RFI characterized using post correlation techniques.

. Total data bandwidth is

$N \times 2B/N_{chan} \times N_{chan} \times N_{pol} \times N_{bits}$

. Parallel data processing.

— Rate in each channel by factor N_{chan}. e.g. with $N_{chan} = 1000$

2 10^{9} $(N/1000)$ $(N_{pol}/2)$ (B/GHz) $(N_{bits}/4)$ bytes/s/chan

3.3. Packetize and Distribute using Switches

. Commercial hardware and protocols.

. Multiple asynchronous data processing

. Distribute the data to beam formers and correlators.

. Flexible programming environment.

. Reuse the hardware for IF processors, beam formers, correlators.

. Flexible routing allows hardware to be maintained and repaired.

. Minimum interruption to array operations

3.4. Beam Formers

. Phased array beams from subset of antennas.

. Sidelobes depend on array geometry.

. Multiple compact targets (pulsars, SETI, RFI, ...)

. Funnel collecting area into expensive backends

. Data must be calibrated into beam formers.

3.5. Correlators

. Versatile mechanism for integrating in the uv domain.

. 40 year experience for calibration and imaging using uv data.

. Data bandwidth for siderial source anywhere in sky:

$N(N+1)/2 \times N_{pol} \times N_{chan} \times N_{bits} \times 2\ sdot \times D_{max}/\lambda$

$10^9\ (N/1000)^2\ (N_{pol}/4)\ (N_{chan}/10^3)\ (N_{bytes}/5)\ (D_{max}/km)\ (\lambda/m)^{-1}$

3.6. Integration at Multiple Phase Centers

. Data rate reduced with further integration.

. Range of fringe rates within the FoV limited by:

— primary beam,

— isoplanatic patch,

— Non coplanar baselines, $\sim sqrt(\lambda/D_{max})$.

. Primary beam imaged by $N_f \sim \lambda D_{max}/D_{ant}^2$ images using 2D FFT.

e.g. ATA, with $D_{ant} = 6$m, $D_{max} = 1$ km,

FoV defined by primary beam $FWHM$, ~ 17 arcmin at $\lambda = 3$ cm,

and by non coplanar baselines at $\lambda = 1$ m.

. CMAC for each baseline and frequency channel, but data rate reduced.

— Data bandwidth imaging the primary beam $FWHM$:

$N(N-1)/2 \times N_{pol} \times N_{chan} \times N_{bits} \times 2\ sdot \times D_{max}/D_{ant}$

$10^8\ (N/1000)^2\ (N_{pol}/4)\ (N_{chan}/10^3)\ (N_{bytes}/5)\ (D_{max}/km)\ (D_{ant}/m)^{-1}$

4. Calibration

. A-priori model used for calibration and imaging.

(In standard paradigm, strong compact sources are primary calibrators,

and self-calibration is used during off-line imaging.)

. Model visibility is calculated as

$V'_{j,k} = exp(2\pi i/\lambda\ r.s_0) \times \Sigma(I \times A \times B \times P \times G \times \exp(2\pi i/\lambda\ r.(s - s_o),$

— $I(s, \nu, p)$ is the model image,

— $A(s, \nu, p)$ is the primary beam response,

— $B(\nu)$ is the instrumental bandpass,

— $P(s, \nu, p)$ is the polarization calibration,

— $G(time, s_0)$ is the gain versus time and phase center.

— $r = (r_j - r_k)$ is the baseline vector, and

— s, ν, and p are the position, frequency and polarization.

— s_o is the phase center for each region of interest.

. Problems:

— the calibrations, A, B, P, and G are complex valued functions,

(can be decomposed into antenna dependent components.)

— Primary beam is product of the antenna voltage patterns.

— Phased array geometry and atmospheric fluctuations make primary beam time variable.

(Even for a single antenna, sidelobes vary due to pointing errors.)

— Wide FoV non isoplanicity.

— Confusing sources in different isoplanatic regions.

. Solution:

— Separately calibrate each phase center.

— Identify bright emission from a-priori images

— Image regions which are of interest or

— Sources whose sidelobes corrupt the regions of interest.

— Integrate data at each phase center; multiply by phase factor $\exp(2\pi i/\lambda\ r.s_o)$.

— A, B, P, and G characterized and applied to the model.

— Self calibration to determine antenna gains $g(t, s_0)$,

— Gains measure tropospheric and ionospheric delays.

— use 3D global model to determine antenna gains.

(function of time for each phase center.)

— Gains include errors in measured A, B, P, and G,

as well as atmospheric amplitude and phase fluctuations at each phase center.

— Gains are not independent for each phase center.

— SNR improved by global model of gain variations across the array.

— Self calibration $\chi^2 = < \Sigma[V \times g_i g_j - V']^2\ /\ \sigma_{ij}^2 >$

(summation over antenna pairs (i, j), frequency channels, time)

— χ^2 accumulated in distributed processors.

— Calibration solves for gains g_i for each time interval and phase center.

— consistent with expected temporal and spatial variations of global model.

— Calibrate the data streams into beam formers and imagers.

— Data streams are delayed to interpolate calibration.

5. Sidelobe subtraction

. Problems:

— Sidelobes of sources outside the regions of interest confuse the images,

— Full FoV cost $\sim \lambda^{1.7} N_{sta} D_{max}^3 / D_{ant}^6$,

N_{sta} = antennas per station. (Perley and Clark 2003).

— non-coplanar baselines, $\sim \lambda N^2 D_{max}^3 / D_{ant}^4$, Cornwell (2004)

— For constant collecting area, $\sim \lambda D_{max}^3 / D_{ant}^8$.

— These scaling relations only apply to full FoV at highest resolution.

(Lonsdale, Doeleman, & Oberoi, 2004; Wright, 2004).

— Larger antennas do not solve the problem.

— Poor *uv* coverage and mosaicing degrade image fidelity.

— Cost for large FoV, N array too expensive.

Solution:

. Stream processing of highly parallel data.

— distributed processors for each region of interest.

— subtract global model from *uv* data stream.

— calibration includes primary beam, bandpass, polarization.

— characterize RFI as function of time, frequency and polarization.

— RFI subtracted from *uv* data stream before beam formers.

6. Imaging

— Parallel processing in distributed architecture.

— Subtract a-priori source model from calibrated uv data.

— Images used to update the global model.

— and improve accuracy of sidelobe subtraction.

— Model and calibration improve as observations proceed.

— Observe until model image is consistent with uv data streams.

— 2D FFT used to image the region around each phase center.

— maximum image size for 2D FFT D_{max}/λ,

— $\sim 10^8$ beam areas on a 1000 km baseline at λ 1 cm.

— Deconvolution minimized by excellent uv coverage for large N.

— Variable sources are inconsistent with the global model.

— χ^2 image identifies tansients.

— Imaging guided in real time by convergence of model and χ^2 image.

— Phase centers can be moved to image regions for science goals,

— and sources discovered in the imaging process.

— and adequately determine the calibration across the FoV.

7. Archive

— *uv* data streams and metadata saved in archive.

— *uv* data streams from archive replayed though imaging system

— improve calibration using best model of sky and phase screen.

8. Proof of concept

— Radical departure from conventional off-line data reduction.

— Image uv data at multiple phase centers.

— Calibrate at each phase center.

— Subtract model at each phase center.

— 2D FFT at each phase center.

— Source subtraction degrades slowly in FoV $\sim sqrt(\lambda/D_{max})$.

— off-line simulation multiple regions are handled sequentially.

— Simulations show we can deconvolve multiple regions from uv data.

— Goal is to develop efficient handling of uv data streams.

— Use existing software in floating point processors.

— Distributed processors for each phase center.

— 10-20,000 uv (1-3 Mbytes/s) on modest sized desktop

9. Epoch of reionization experiment

— (Backer and Bradley, 2005)

— 150-200 MHz, 513 spectral channels sampled at 0.1 Hz,

— Image entire field of view

— *uv* data phase rotated to Cygnus A and Cas A

— Antenna positions fitted over a limited HA range.

— Self-calibrate at each phase center.

— No correction for primary beam response or polarization

— Dynamic range ~ 100

— Spectral dynamic range ~ 1000

10. Data Structures

— Block floating used in the hardware.

— MIRIAD *uv* data is stream of scaled 16-bit integers.

— Metadata is stream of named variables and values.

11. Hardware prototype

— Multipurpose computing platform for radio telescope DSP.

— FPGA enable wide range of radio astronomy applications.

— Current design 5 to 10 years from concept to production.

— BEE2 250 10^9 CMAC/s

— memory bandwidth 12 GB/s

— I/O bandwidth 360 Gb/s

— System design philosophy treats boards as modular DSP resource.

— Flexible interconnect architecture allows reconfiguration for multiple applications.

— Programming model allows focus on application rather than the hardware.

— Software survives by using a technology independent design flow.

— Programmable "digital lens" for radio astronomy.

12. Summary

. Calibration and imaging integrated with hardware.

. FX correlators and beam formers.

. Stream data processing

. Flexible programming environment.

. Narrow frequency channels and short integration times.

. Multiple delay centers within large FoV.

. Simultaneous imaging at multiple phase centers.

. Calibration in real time using global model.

. Calibration feedback into beam formers and imagers.

. Subtract global model from *uv* data before imaging.

. Difference images update global a-priori model

. Model becomes final image when observations completed.

. Calibrated images as normal output.

Table 1: Limits on the Field of View and Sampling Rates for the ATA and SKA. D_{max} is the maximum antenna separation. D_{ant} is the antenna diameter. λ/D_{ant} is the primary beam FWHM. $sqrt(\lambda/D_{max})$ is the limit to the image size imposed by non-coplanar baselines. $N_f \sim \lambda D_{max}/D_{ant}^2$ is the number of image regions needed, using a 2D FFT, to cover the primary beam $FWHM$. c/D_{max} is an upper limit to the channel width to avoid bandwidth smearing on the longest baseline without delay tracking. $Fringe$ is the maximum rate of change of the cross correlation, and $Nyquist$ is the sample rate within the primary beam $FWHM$.

λ [m]	D_{max} [km]	D_{ant} [m]	λ/D_{max} [arcsec]	λ/D_{ant} [arcmin]	$sqrt(\lambda/D_{max})$ [arcmin]	N_f	c/D_{max} [kHz]	$Fringe$ [Hz]	$Nyquist$ [Hz]
1.00	1	6	206.26	572.9	108.7	27.8	300	0.07	0.02
0.21	1	6	43.32	120.3	49.8	5.8	300	0.35	0.02
0.03	1	6	6.19	17.2	18.8	0.8	300	2.42	0.02
1.00	1	12	206.26	286.5	108.7	6.9	300	0.07	0.01
0.10	1	12	20.63	28.6	34.4	0.7	300	0.73	0.01
0.01	1	12	2.06	2.9	10.9	0.1	300	7.27	0.01
1.00	10	12	20.63	286.5	34.4	69.4	30	0.73	0.12
0.10	10	12	2.06	28.6	10.9	6.9	30	7.27	0.12
0.01	10	12	0.21	2.9	3.4	0.7	30	72.7	0.12
1.00	100	12	2.06	286.5	10.9	694.4	3	7.27	1.21
0.10	100	12	0.21	28.6	3.4	69.4	3	72.7	1.21
0.01	100	12	0.02	2.9	1.1	6.9	3	727.	1.21
1.00	1000	12	0.206	286.5	3.4	6944.	0.3	72.7	12.12
0.10	1000	12	0.021	28.6	1.1	694.4	0.3	727.	12.12
0.01	1000	12	0.002	2.9	0.3	69.4	0.3	7270.	12.12
1.00	1000	25	0.206	137.5	3.4	1600.	0.3	72.7	5.82
0.10	1000	25	0.021	13.8	1.1	160.	0.3	727.	5.82
0.01	1000	25	0.002	1.4	0.3	16.	0.3	7270.	5.82

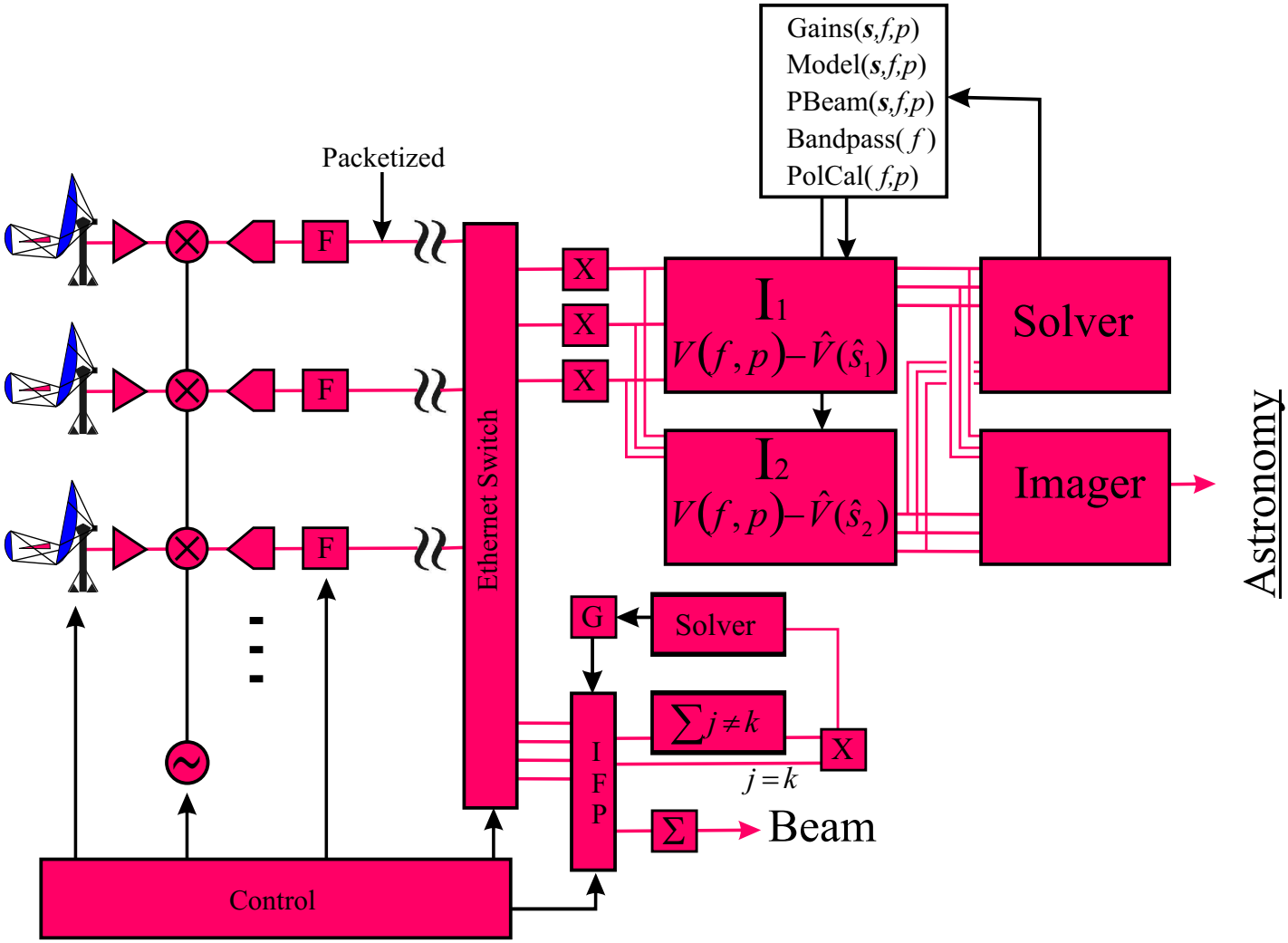

Fig. 1.— Data flow from telescopes to images.

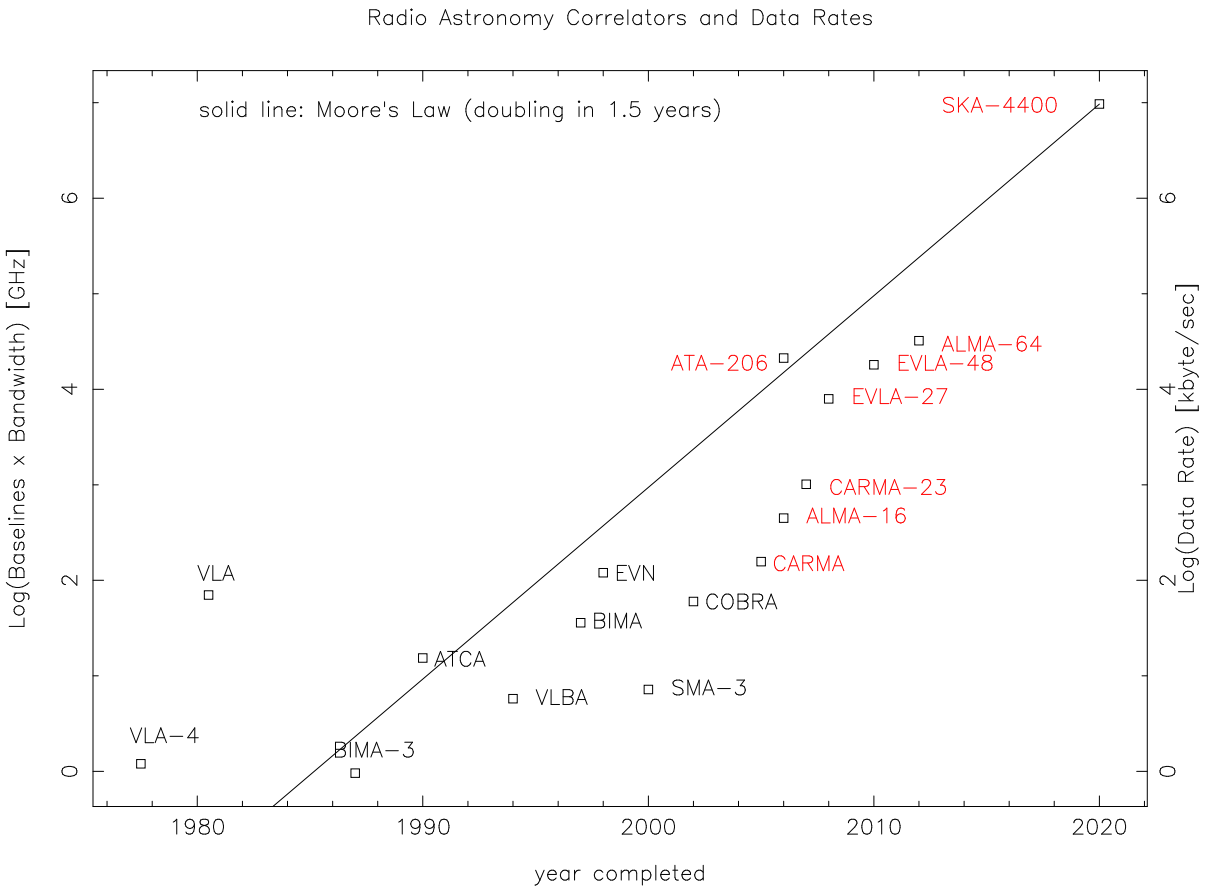

Fig. 2.— Radio Astronomy Correlators

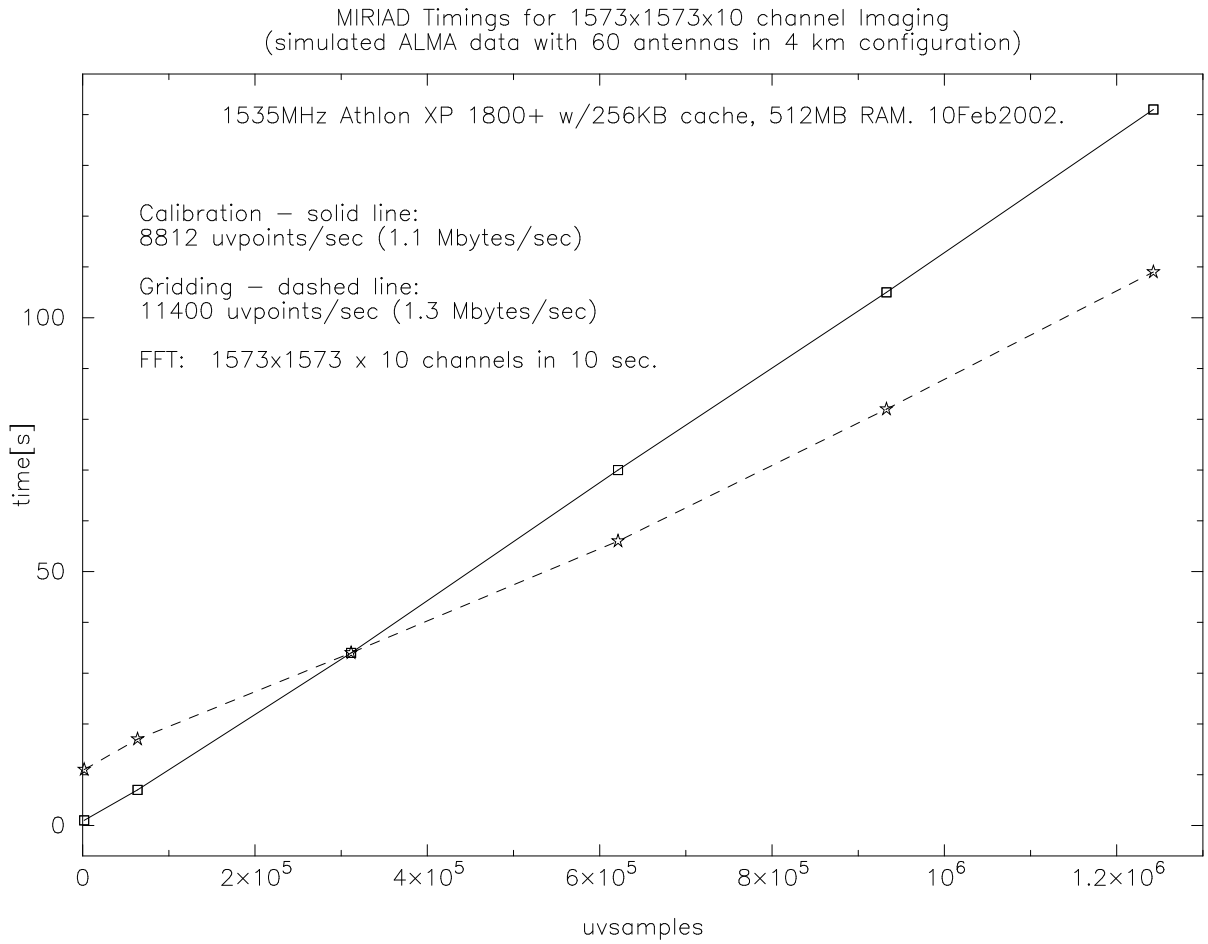

Fig. 3.— Multichannel Calibration and Imaging

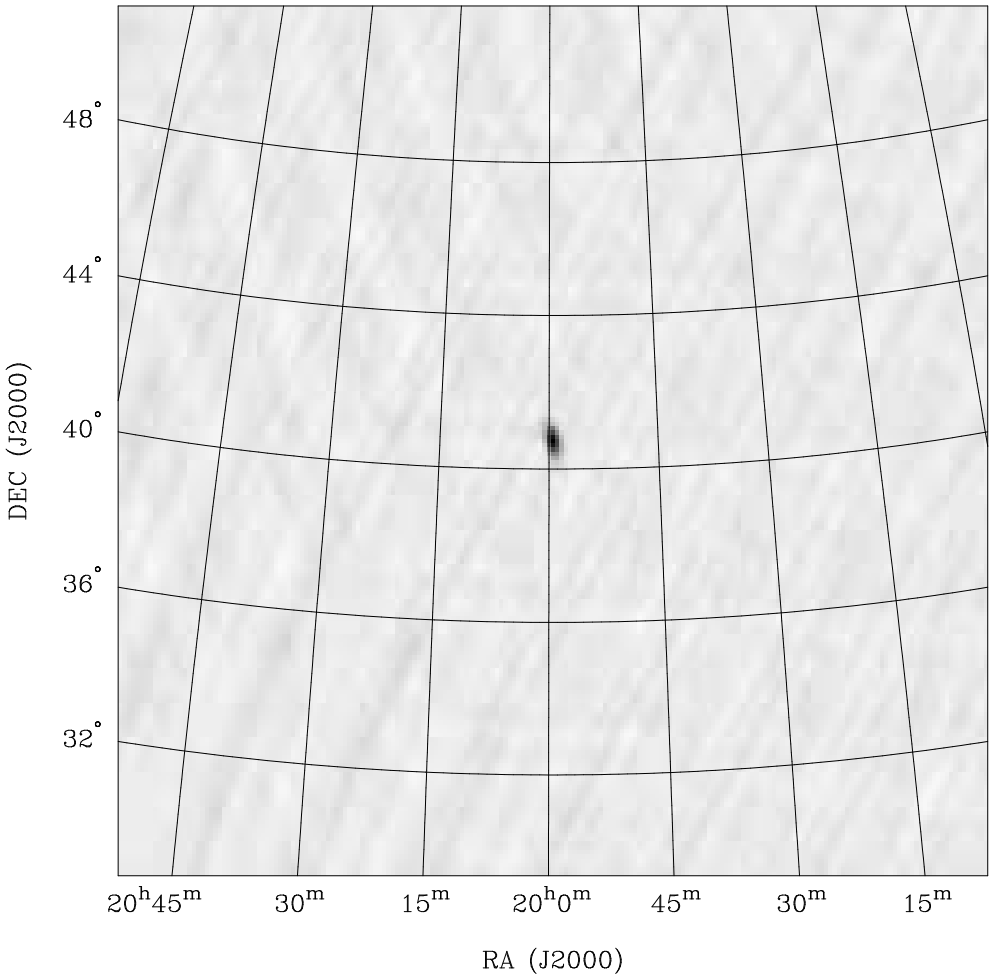

Fig. 4.— Cygnus Image at 175 MHz from 4-dipole array

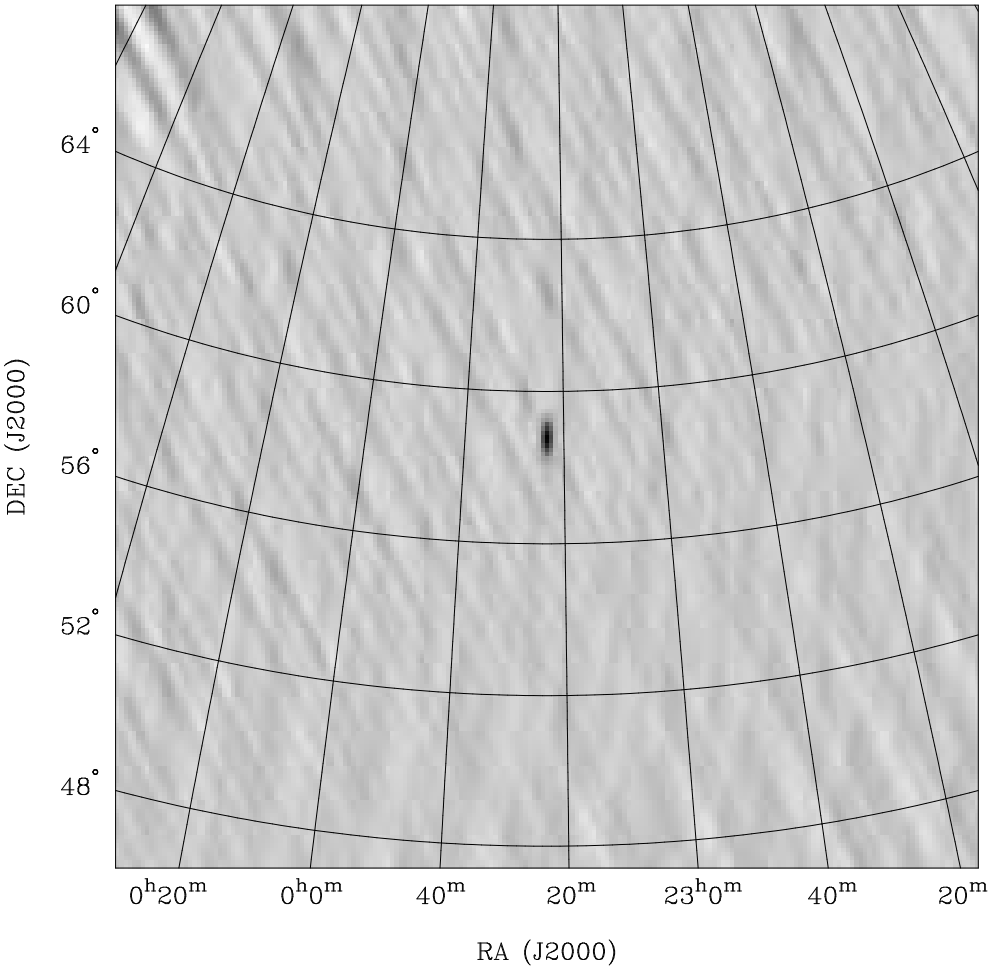

Fig. 5.— Cas A Image at 175 MHz from 4-dipole array

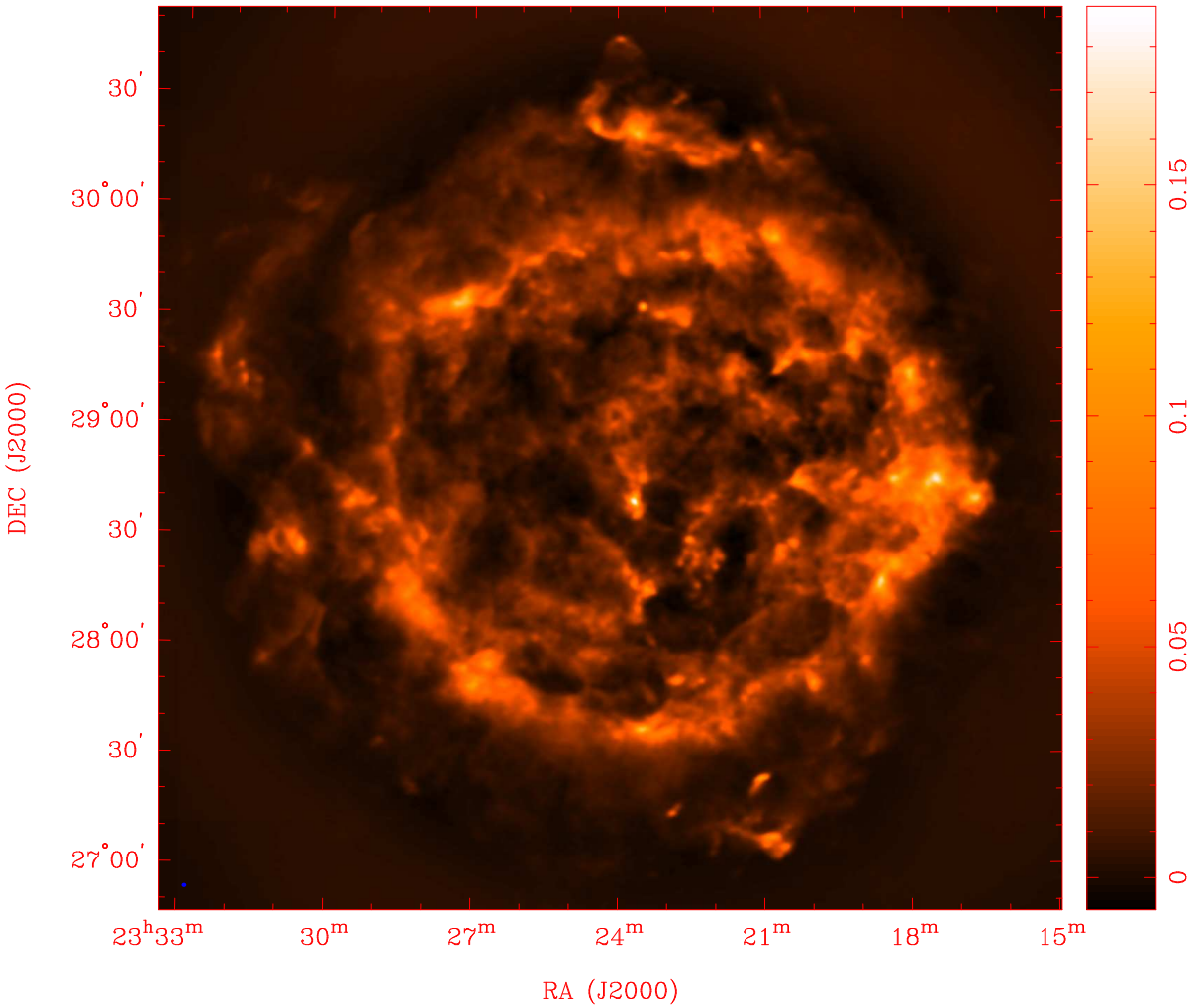

Fig. 6.— A mosaic MFS Image of CASA scaled up 40 times real size, imaged with the ATA at 1.42 GHz. The image is 4 degrees on a side. The synthesised beam FWHM, 77 x 78 arcsec is shown in the lower left corner.